LETTERS

nature cell biology

A common lipid links Mfn-mediated mitochondrial fusion and SNARE-regulated exocytosis

Seok-Yong Choi[1,2], Ping Huang[2,5], Gary M. Jenkins[2,5], David C. Chan[3], Juergen Schiller[4] and Michael A. Frohman[1,2,6]

Fusion of vesicles into target membranes during many types of regulated exocytosis requires both SNARE-complex proteins and fusogenic lipids, such as phosphatidic acid. Mitochondrial fusion is less well understood but distinct, as it is mediated instead by the protein Mitofusin (Mfn). Here, we identify an ancestral member of the phospholipase D (PLD) superfamily of lipid-modifying enzymes that is required for mitochondrial fusion. Mitochondrial PLD (MitoPLD) targets to the external face of mitochondria and promotes trans-mitochondrial membrane adherence in a Mfn-dependent manner by hydrolysing cardiolipin to generate phosphatidic acid. These findings reveal that although mitochondrial fusion and regulated exocytic fusion are mediated by distinct sets of protein machinery, the underlying processes are unexpectedly linked by the generation of a common fusogenic lipid. Moreover, our findings suggest a novel basis for the mitochondrial fragmentation observed during apoptosis.

Parallel dimerization of vesicle- and target-SNARE coiled–coil proteins tethers exocytic vesicles to the plasma membrane and drives fusion of the opposing bilayer membranes[1]. Although the SNAREs suffice to mediate detectable levels of fusion in isolation[2], increasing their efficiency to physiological levels during regulated exocytosis requires additional factors in many settings, including manipulation of the lipid environment through the production of acidic fusogenic lipids such as phosphatidic acid and phosphatidylinositol 4,5-bisphosphate (PtdIns(4,5)P_2) by the enzymes PLD[3,4] and PtdIns(4,5)P_2 kinase[5]. In contrast, fusion of mitochondria depends on Mfn (also known as Fzo)[6–8], which tethers opposing mitochondrial outer membranes together through anti-parallel dimerization of a coiled–coil domain[9]. In addition, the GTPase domain of Mfn performs an unknown but vital action in the fusion process[8,10]. The mechanism through which Mfn promotes fusion of the outer membrane is not well understood, nor have additional components of the mammalian fusion machinery required for this step been identified. Here, we describe the unexpected finding that generation of phosphatidic acid, a lipid shown to facilitate specialized SNARE-complex driven vesicular fusion events in yeast[11] and mammals[3,4], is a key component in Mfn-mediated mitochondrial fusion.

BLAST search of the human genome using the PLD catalytic-site HKD motif[12] uncovered several previously undescribed members of the PLD superfamily, including a widely expressed protein (see Supplementary Information, Fig. S1) denoted MitoPLD, which encoded a predicted mitochondrial localization sequence (MLS; Fig. 1a and see Supplementary Information, Fig. S1). Unlike the classic mammalian isoforms PLD1 and PLD2 that encode PX, PH and PtdIns(4,5)P_2-binding protein domains that mediate localization, and two copies of the HKD motif that juxtapose to form the catalytic site[13], MitoPLD encodes solely a single HKD half-catalytic site. Phylogenetic analysis revealed that MitoPLD is a divergent and ancestral family member most similar to bacterial cardiolipin synthase and to bacterial endonuclease Nuc, a PLD superfamily member that also encodes a single half-catalytic site and dimerizes to function (see Supplementary Information, Fig. S1)[14]. Confocal microscopy analysis of MitoPLD expressed as a carboxy-terminal fusion protein with EGFP confirmed its localization to mitochondria (Fig. 1b), and the MLS was found to be necessary and sufficient for localization (Fig. 1c, d). Most nuclear-encoded proteins targeted to the mitochondria through an amino-terminal MLS enter into the matrix through the protein import apparatus Tom (translocase of the outer membrane), and while doing so, undergo processing that removes the MLS[15]. However, western blot analysis of overexpressed MitoPLD revealed full-length rather than processed protein (Fig. 1e), suggesting that the MLS, which also scored as a potential transmembrane domain (see Supplementary Information, Fig. S1), may be retained and serve to anchor MitoPLD to the outer membrane surface, as is the case for Tom20 (ref. 15). This possibility was addressed using protease surface digestion of intact mitochondria (Fig. 1f and see Supplementary Information, Fig. S2), which confirmed the topology. Split-Venus complementation (Fig. 1g; which tests potential protein–protein interactions by assaying for reassembly of amino- and carboxy-terminal fragments of Venus fluroescent protein appended

[1]Graduate Program in Molecular and Cellular Biology and [2]Department of Pharmacology, Center for Developmental Genetics, Stony Brook University, Stony Brook, NY 11794–5140, USA. [3]Division of Biology, Beckman Institute, California Institute of Technology, Pasadena, CA 91125, USA. [4]University of Leipzig, Medical Faculty, Institute of Medical Physics and Biophysics, Härtelstr. 16/18, 04107 Leipzig, Germany. [5]These authors contributed equally to this work.
[6]Correspondence should be addressed to M.A.F. (e-mail: Michael@pharm.stonybrook.edu)

Received 26 June 2006; accepted 10 August 2006; published online 8 October 2006; DOI: 10.1038/ncb1487

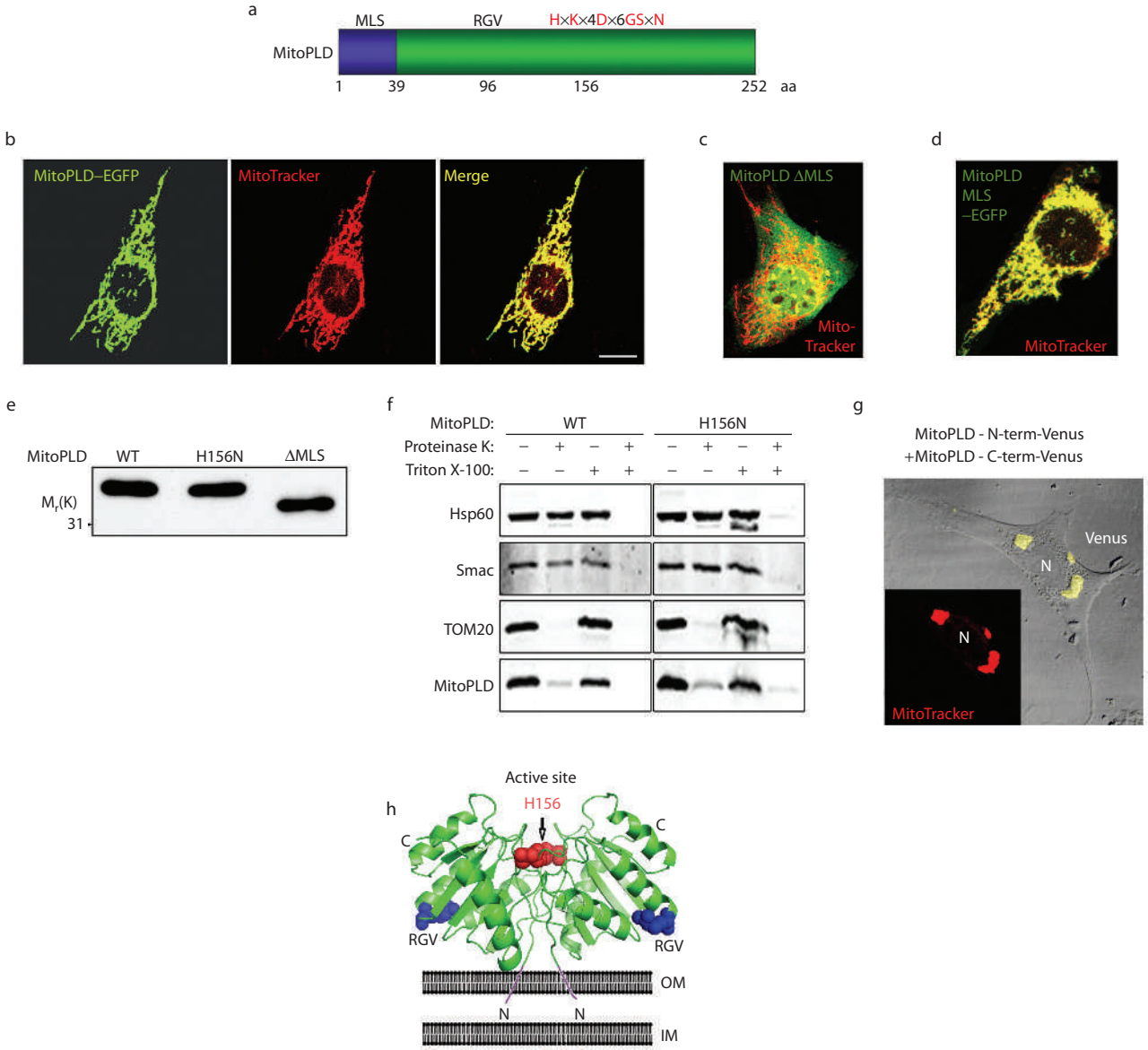

Figure 1 Dimerized MitoPLD localizes to the mitochondrial exterior. (**a**) Schematic representation of the MitoPLD protein. HxKx4Dx6GSxN, HKD motif; RGV is a motif of unknown function conserved in this subset of the PLD superfamily (see Supplementary Information, Fig. S1). MLS, mitochondrial localization sequence. (**b**–**d**) Confocal microscopy analysis of NIH3T3 cells transfected with plasmids expressing MitoPLD C-terminally fused to EGFP (**b**), MitoPLD lacking the MLS (ΔMLS; **c**) or the MitoPLD MLS fused to EGFP (**d**). The scale bar represents 10 μm. Mitochondria are indicated by MitoTracker Deep Red. (**e**) Western blot analysis of HEK293 cells transfected with plasmids expressing epitope-tagged wild-type (WT), mutant (H156N), or ΔMLS-MitoPLD. (**f**) Mitochondria purified from cells expressing Flag-tagged wild-type MitoPLD or MitoPLD^{H156N} were exposed to proteinase K in the presence or absence of Triton X-100. Hsp60 (a mitochondrial matrix protein), Smac (an inter-membrane space protein) and TOM20 (which projects from the outer membrane) were visualized using commercial antisera. (**g**) MitoPLD alleles fused individually to the N- or C-halves of Venus fluorescent protein were transiently cotransfected into NIH3T3 cells. The observance of yellow fluorescence (reconstituted Venus) signifies that the MitoPLD monomers dimerize. Mitochondria are indicated by MitoTracker Deep Red. (**h**) Schematic representation of MitoPLD extra-mitochondrial dimerization and proposed outward-facing orientation generated by threading human MitoPLD onto the published coordinates for bacterial Nuc[14]. The transmembrane domain (magenta) was not contained within the region modelled. MitoPLD is shown oriented with respect to the outer (OM) and inner (IM) mitochondrial membranes. C, N; C- and N-termini. H156 is the key catalytic-site residue.

to the candidate interacting proteins), and coimmunoprecipitation (see Supplementary Information, Fig. S2) confirmed that MitoPLD dimerizes *in vivo* (the abnormal mitochondrial morphology is discussed in Fig. 2). However, modelling of the resulting N-terminally tethered dimer on bacterial Nuc[14] and PLD[16] suggested that the lipid-hydrolysing catalytic pocket should paradoxically be oriented away from the mitochondrial outer membrane surface (Fig. 1h), raising the intriguing question of what function this presumed enzyme undertakes.

An answer was suggested by the phenotype observed with moderate overexpression of MitoPLD (as opposed to the lower level of expression shown in Fig. 1b), which consisted of aggregation of the normally well-distributed tubular mitochondria (Fig. 2a, control) into a seemingly continuous giant peri-nuclear mitochondrion (Fig. 2a, MitoPLD). Specificity of the phenotype and confirmation that MitoPLD is a *bona fide* enzyme was demonstrated by overexpressing a mutant allele, H156N, in which the key catalytic histidine had been converted to an

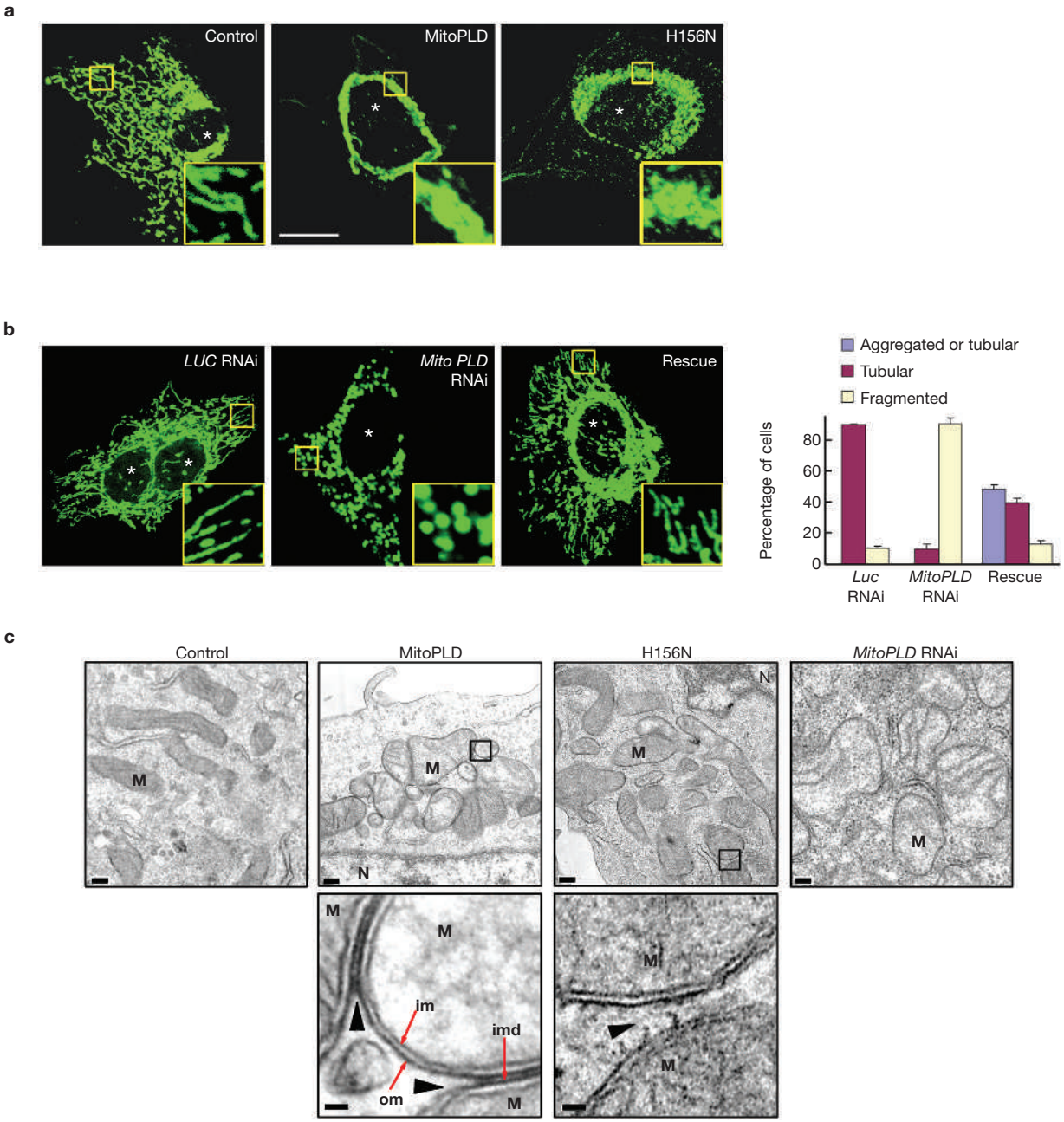

Figure 2 MitoPLD aggregates mitochondria. (**a**) Confocal microscopy analysis of NIH3T3 cell lines stably transfected with mifepristone-inducible expression plasmids for wild-type or mutant (H156N) alleles of Flag-tagged MitoPLD that were induced for 24 h and stained with anti-cytochrome *c* antibodies. The scale bar represents 10 μm. Insets represent magnifications of the boxed areas. The asterisks indicate the nucleus. (**b**) HeLa cells stably expressing RNAi targeting *luciferase* (*Luc*) or *MitoPLD* (80–90% knockdown, based on real-time RT-PCR) were imaged using transient transfection of mito-EGFP. A representative cell after transfection of the *MitoPLD* RNAi-expressing cells with RNAi-resistant *MitoPLD-EGFP* is shown (rescue). The bar graph shows the relative frequency of mitochondrial morphologies ($n = 3$ independent experiments; 300 cells scored per experiment; mean ± s.d. is shown). (**c**) Electron microscopy analysis of control, wild-type and mutant MitoPLD-overexpressing, and RNAi-expressing cells. The boxed areas are magnified in the lower panels. The scale bars represent 200 nm in the top row, and 25 nm in the bottom row. M, mitochondrion; N, nucleus; imd, inter-mitochondrial distance.

asparagine, which in all PLD family members studied to date results in complete loss of catalytic activity[13]. In this case, the normal mitochondrial tubular morphology was again disrupted, but was replaced instead by a collection of non-contiguous mitochondrial fragments (Fig. 2a, H156N). As MitoPLD dimerizes, this construct should be an effective dominant–negative allele. To confirm the requirement of MitoPLD for normal mitochondrial morphology, cell lines stably expressing short hairpin RNA (shRNA) directed against MitoPLD were generated. The cell lines similarly exhibited mitochondrial fragmentation, and as a measure of specificity of the RNA interference (RNAi) targeting, mitochondrial fragmentation could be rescued by expression of an RNAi-resistant *MitoPLD* cDNA (Fig. 2b). Electron microscopy analysis (Fig. 2c) confirmed and extended these findings; rather than being a continuous mitochondrion, the mitochondria in cells overexpressing MitoPLD were

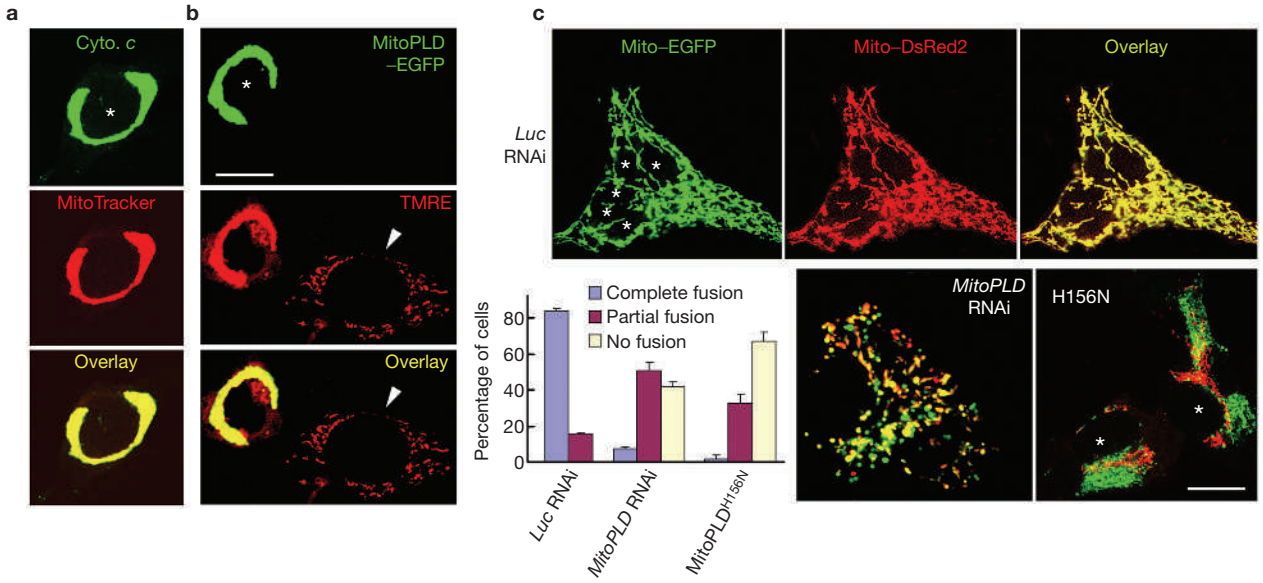

Figure 3 MitoPLD is required for fusion. (**a**) Confocal analysis of NIH3T3 cells stably overexpressing Flag-tagged MitoPLD, labelled with MitoTracker Deep Red and immunostained using anti-cytochrome *c* antibody. (**b**) NIH3T3 cells transiently transfected with MitoPLD-EGFP and labelled with tetramethylrhodamine ethyl ester (TMRE) demonstrate mitochondrial membrane potential ($\Delta\Psi_m$). Arrowhead, non-transfected cell. The scale bar represents 10 μm. (**c**) Pools of cells individually expressing Mito–EGFP or Mito–DsRed2 were coplated, fused using PEG 1500 and imaged 7 h later. Top row, Individual and merged channels are shown for a representative HeLa cell stably expressing *Luc* RNAi. Merged examples from fusion experiments conducted using *MitoPLD* RNAi-expressing HeLa cells or NIH3T3 cells induced to express dominant–negative MitoPLD^{H156N} are shown: partial fusion is shown for *MitoPLD* RNAi and no fusion for the H156N-expressing cells. The bar graph shows the relative frequencies of full, partial and no fusion observed for each cell line ($n = 3$).

actually aggregated into a compound structure that was not resolvable at the confocal microscopy level. Strikingly, a regular and uniform distance (5.9 ± 1.8 nm, $n = 20$) was observed separating the opposing outer membranes of distinct mitochondria. In contrast, non-uniform and much larger separating distances were observed in cells expressing dominant–negative MitoPLD^{H156N} or *MitoPLD* RNAi. Cells stably expressing elevated levels of MitoPLD or MitoPLD^{H156N} remained viable, proliferated normally, did not exhibit translocation of cytochrome *c* into the cytoplasm (Fig. 3a) and maintained mitochondrial membrane potential ($\Delta\Psi_m$;Fig. 3b); hence, the respective altered mitochondrial morphologies did not seem to trigger or result from apoptosis or major alterations in cell homeostasis. Taken together, these altered morphologies suggested that MitoPLD may function in mitochondrial fusion. To address this, a mitochondrial fusion assay[17] was performed and we found that cells deficient in MitoPLD or expressing the MitoPLD^{H156N} dominant–negative allele exhibit dramatically decreased levels of fusion (Fig. 3c).

Current models for mitochondrial fusion propose that the process is initiated by a tethering step carried out by Mfn, which juxtaposes opposing mitochondrial outer membranes approximately 16 nm apart[9]. Electron microscopy findings confirmed the separating distance reported for Mfn1 (16.4 ± 2.4 nm, $n = 20$), suggesting that MitoPLD-mediated aggregation (Figs 2c and 4a) brings the opposing outer membrane leaflets closer together, which can be observed even at the resolution level of confocal microscopy (Fig. 4b). This observation suggested that MitoPLD may function downstream of Mfn-mediated tethering to perform a subsequent step in the fusion process. To investigate this possibility, the epistatic relationship between Mfn-mediated tethering and MitoPLD-mediated aggregation was examined. There are two mammalian isoforms of Mfn, Mfn1 and Mfn2. Cells lacking Mfn1 have reduced rates of fusion, whereas cells lacking both Mfn1 and Mfn2 exhibit no fusion; both types of cells are characterized by fragmented mitochondria (Fig. 4c)[18,19]. MitoPLD was transfected into these cell lines and conversion of the fragmented mitochondria into aggregated mitochondria was observed in the absence of Mfn1, but not in the absence of both Mfn1 and Mfn2 (Fig. 4c). These findings demonstrate that MitoPLD-induced aggregation requires at least low levels of Mfn activity. Conversely, transfection of the C-terminal portion of Mfn1 (tether; amino acids 331–741), which suffices to mediate tethering[9], into cells expressing the dominant–negative MitoPLD^{H156N} allele or into *MitoPLD* RNAi cells, succeeded in generating mitochondria tethered at a distance generally similar to that observed after transfection of the tether into wild-type cells (Fig. 4d), suggesting that Mfn tethering does not require MitoPLD activity. Furthermore, transfection of the Mfn1 tether into cells overexpressing wild-type MitoPLD resulted in a separating distance similar to that observed when MitoPLD alone was overexpressed (Fig. 4d), suggesting that the MitoPLD aggregation phenomenon dominates over the Mfn-induced tethering action. It is not known whether MitoPLD action precedes, follows or affects the action of the Mfn GTPase domain. Taken together, these results suggest that MitoPLD functions downstream of Mfn-mediated tethering. We propose that MitoPLD functions in *trans* to modify the lipid surface of the opposing mitochondrial outer membrane and that this modification occurs at physiologically significant rates only if Mfn tethers the respective mitochondria in opposition for an adequate period of time. However, this model raises issues regarding the mechanism of MitoPLD action.

The MitoPLD protein sequence is most similar to the bacterial endonuclease Nuc and bacterial cardiolipin synthase (but not to eukaryotic cardiolipin synthase, which is a member of an unrelated gene family). Neither nuclease activity nor cardiolipin synthetic activities could be detected (see Supplementary Information, Fig. S3); however, using

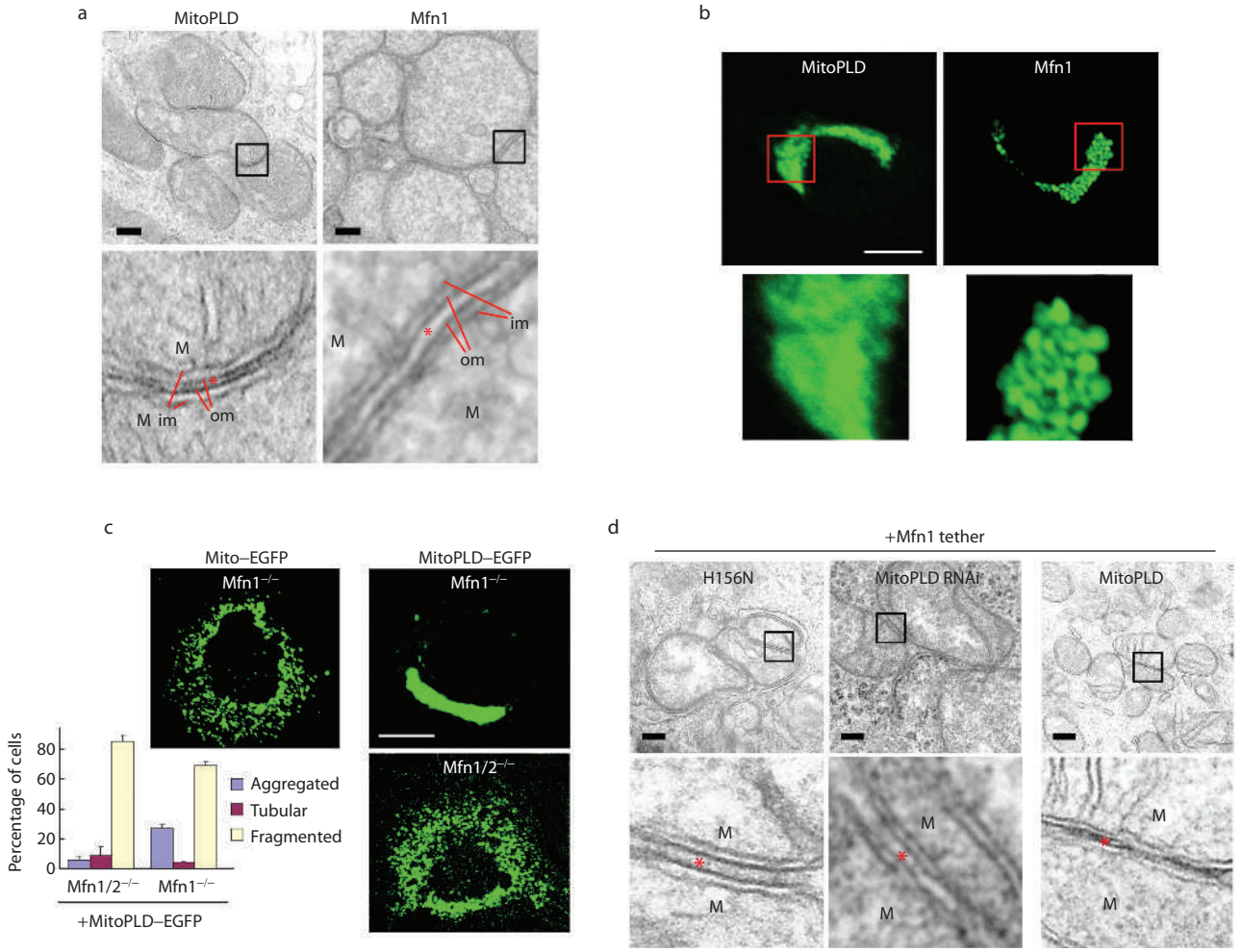

Figure 4 MitoPLD functions downstream of Mfn. (**a**, **b**) Electron microscopy and confocal microscopy analysis of NIH3T3 cell lines inducibly overexpressing MitoPLD or the Mfn1 tether (aa 331–741). The boxed areas are magnified in the lower panels. The asterisks indicate intervening distance between adjacent double-membrane mitochondria (MitoPLD, 5.9 ± 1.8 nm; Mfn1, 16.4 ± 2.4 nm; $n = 20$). The scale bars represent 200 nm. (**c**) Mouse embryonic fibroblasts (MEFs) lacking Mfn1 (*Mfn1*$^{-/-}$) or lacking both Mfn1 and Mfn2 (*Mfn1/2*$^{-/-}$) were transfected with EGFP-tagged MitoPLD. Mitochondrial morphologies were tabulated in three independent experiments ($n = 300$ in total for each experimental condition). *Mfn1*$^{-/-}$ MEFs transfected only with Mito–EGFP are shown as a control. The scale bar represents 10 μm. The graph shows the relative frequencies of aggregated, tubular and fragmented mitochondria observed for each cell line ($n = 3$). (**d**) Electron microscopy analysis of NIH3T3 cells inducibly overexpressing wild-type or dominant–negative (H156N) MitoPLD or *MitoPLD* RNAi HeLa cells, transfected with a plasmid expressing the Mfn1 tether. Representative images are shown. Cells expressing both the Mfn1 tether and H156N exhibited a distance of 15.8 ± 3.1 nm between the outer membranes ($n = 20$). The boxed areas are magnified in the lower panels.

one-dimensional (Fig. 5a) and two-dimensional (Fig. 5b) thin layer chromatography (TLC), an altered profile of mitochondrial lipids was observed after MitoPLD overexpression, consisting of a decrease in cardiolipin (19 ± 6% of control levels, $n = 3$) and an increase in phosphatidic acid (199 ± 58% of control levels, $n = 3$). Small decreases in phosphatidylethanolamine were sometimes noted and limited hydrolysis of other phopholipids cannot be excluded. No changes in the levels of cardiolipin or phosphatidic acid were noted in cells overexpressing the MitoPLD dominant–negative H156N allele or in *MitoPLD* RNAi cells (Fig. 5b and data not shown), demonstrating linkage of the altered profile to MitoPLD enzymatic activity. Cardiolipin levels were also examined in cells overexpressing Mfn1. No decrease in cardiolipin was observed, demonstrating that mitochondrial aggregation *per se* does not deplete cardiolipin and thus providing specificity for the decrease observed when MitoPLD was overexpressed. Finally, a direct demonstration of MitoPLD hydrolysis was achieved using purified recombinant protein (Fig. 5c) in combination with liposomes containing labelled cardiolipin. In the experiment shown in Fig. 5d, wild-type MitoPLD hydrolysed 8.4% of the labelled cardiolipin to generate phosphatidic acid, whereas no phosphatidic acid generation was observed in the absence of input protein or in the presence of catalytically inactive MitoPLD^{H156N}.

From a biochemical perspective, the identification of MitoPLD as an enzyme that hydrolyses cardiolipin to generate phosphatidic acid is not unreasonable, given its similarity to a bacterial cardiolipin synthase, which mediates the same reaction in the reverse direction. Moreover, cardiolipin-hydrolysing activities have previously been demonstrated for a bacterial PLD[20]. From a mitochondrial perspective, however, this could be considered a surprising finding, as cardiolipin is found predominantly on the inner leaflet of the mitochondrial inner membrane, whereas we present evidence here that MitoPLD localizes to the outer leaflet of the outer membrane. The outer membrane does contain 10–20% of the total mitochondrial cardiolipin[21,22], most of which is in the outer leaflet[22] at

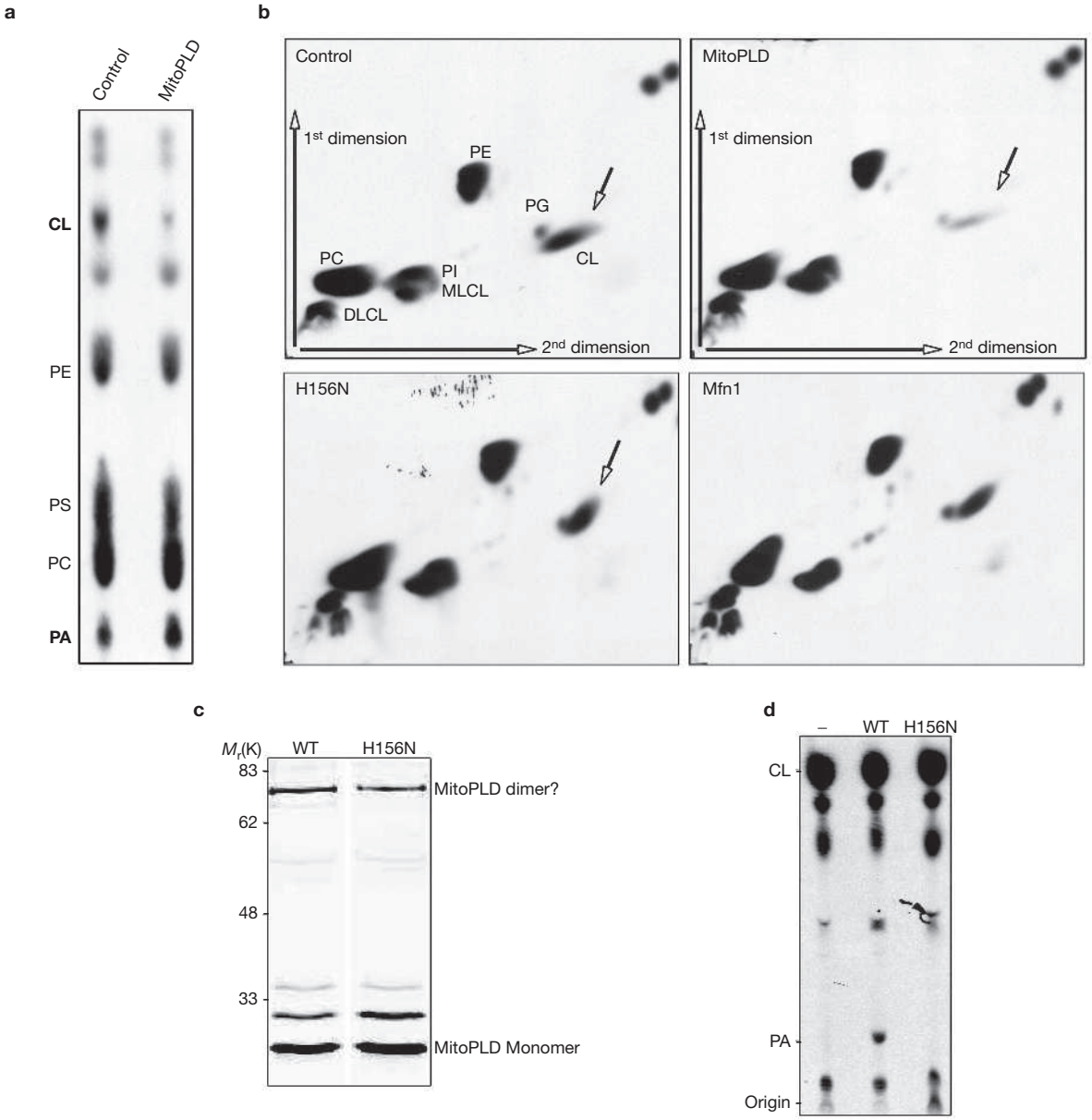

Figure 5 MitoPLD hydrolyses cardiolipin to generate phosphatidic acid. (**a**) An NIH3T3 cell line stably transfected with a mifepristone-inducible expression plasmid for wild-type Flag-tagged MitoPLD was cultured with or without mifepristone for 24 h and the mitochondria processed for one-dimensional TLC analysis. PA, phosphatidic acid; CL, cardiolipin; PE, pho sphatidylethanolamine; PS, phosphatidylserine; PC, phosphatidylcholine. (**b**) Two dimensional TLC analysis of mitochondria from NIH3T3 cell lines induced to express wild-type MitoPLD, catalytically inactive MitoPLD^{H156N}, or Mfn1. DLCL, dilysocardiolipin; MLCL, monolysocardiolipin; PI, phosphatidylinositol. The arrow indicates cardiolipin. Images are representative of three independent experiments. (**c**) Generation of purified MitoPLD using baculoviral expression and His-tag purification as visualized using Coomassie blue staining. (**d**) Direct hydrolysis of cardiolipin by MitoPLD. Wild-type and catalytically inactive purified MitoPLD protein (or no input protein) were incubated with liposomes containing ^{3}H-labelled cardiolipin at 37 °C for 30 min in the standard buffer used for classical *in vitro* PLD assays[13], following which the lipids were extracted and analysed by TLC.

inner membrane–outer membrane contact sites. Moreover, cardiolipin has been shown to translocate in a regulatable manner from the inner membrane to the outer membrane[21], and as cardiolipin remodelling takes place on the mitochondrial exterior or in the endoplasmic reticulum[23], most cardiolipin presumably transits through the outer membrane post-synthesis before returning to the mitochondrial interior. Thus, an overexpressed outer membrane cardiolipin-modifying enzyme should eventually be able to gain access to most of the mitochondrial cardiolipin. Our findings have two important implications: first, they suggest that mitochondrial fusion takes place in the regions overlying contact sites, which is an attractive idea but one for which support has not previously been generated; second, they suggest a novel mechanism to link the mitochondrial fragmentation observed during apoptosis to the apoptotic process. The rate of fusion is known to decrease during apoptosis[24]. We propose that this may ensue from a combination of sequestration by tBid (a caspase-8-cleaved Bid fragment that triggers mitochondrial fragmentation) and/or decreased cardiolipin availability subsequent to apoptosis-induced cardiolipin deacylation[25] or cytochrome *c*-mediated cardiolipin peroxidation[26]. This would lead to decreased MitoPLD production of phosphatidic acid and an ensuing decrease in the rate of

fusion, which would cause fragmentation if the level of fission remained unchanged. An analogous mechanism exists in yeast, where cell-cycle arrest-triggered fragmentation is mediated by the ubiquitination and downregulation of Mfn (also known as Fzo1)[27].

Here, we show a requirement for MitoPLD-mediated generation of phosphatidic acid in mitochondrial fusion. Thus far, we have uncovered no other roles for MitoPLD in the fusion process. Coimmunopreciptation analysis did not reveal an interaction between MitoPLD and Mfn1 or Mfn2, and levels of Mfn 1 and 2 protein expression were not altered in cells overexpressing wild-type or MitoPLD^{H156N}, or in *MitoPLD* RNAi cells (see Supplementary Information, Fig. S2, and data not shown). The requirement for production of phosphatidic acid is reminiscent of the requirement for classic PLD-dependent generation of phosphatidic acid in SNARE-mediated fusion of secretory vesicles with the plasma membrane during many types of regulated exocytosis[3,4] and during sporulation in yeast[11]. Taken together, these findings reveal a common requirement for a specific manipulation of the lipid environment despite the lack of conservation of the associated protein machinery and mechanism of action. The role of phosphatidic acid remains undetermined — it may facilitate fusion by generating negative curvature in the opposing bilayers, by recruiting or activating other key proteins or enzymes, or by being further converted to other fusogenic lipids (such as diacylglycerol). Interestingly, phosphatidic acid has been shown to recruit Spo20, the yeast homologue of the mammalian t-SNARE 25, to sites of vesicle fusion through direct interaction[28], and to accelerate the rate of mammalian SNARE-driven vesicle fusion *in vitro*[29].

Mutations in Mfn2 are the most frequent cause of Charcot-Marie-Tooth type 2A disease, an inherited peripheral neuropathy[30]. Although the physiological consequence of MitoPLD deficiency is presently unknown, some possibilities are suggested by the localization of the human *MitoPLD* gene to 17p11.2 in a region frequently duplicated in Charcot-Marie-Tooth 1A disease and deleted in Smith-Magenis syndrome[31], the latter of which is characterized, in part, by a peripheral neuropathy thought to ensue from heteroinsufficiency of an unknown gene in the region. □

METHODS

General reagents. Cell culture media, DMEM, Opti-MEM-I, and LipofectAMINE Plus were from Invitrogen (Carlsbad, CA). MitoTracker Deep Red 633 was purchased from Molecular Probes (Carlsbad, CA). All other reagents were of analytical grade unless otherwise specified.

DNA manipulation. An EST clone (GenBank accession number, BI562496; IMAGE consortium clone number, 5298498) was identified through the tBlastn search with an HKD motif against the human EST database. The coding sequence of *MitoPLD* was PCR-amplified from the IMAGE consortium clone using primers 5′-CTAGCTCGAGACCATGGGACGGTTGAGTTGG-3′ and 5′-CGGATCCCG GGTTTGGCTTTCGCTGGAG-3′ terminating with *Xho*I and *Xma*I restriction sites, respectively. The resulting PCR product was subcloned in-frame into the *Xho*I and *Xma*I sites of pEGFP-N1 (Clontech, Mountain View, CA). MitoPLD^{H156N} was generated using the QuickChange Site-directed Mutagenesis kit (Stratagene, La Jolla, CA) with primers 5′-CCCAGGCTACATGAATCACAAGTTTGC-3′ and 5′-GCAAACTTGTGATTCATGTAGCCTGGG-3′ (mutations are underlined). The sequences of all plasmids generated were confirmed by sequencing.

Cell culture and transfection. Cells were maintained in DMEM supplemented with 10% calf serum (Hyclone, Logan, UT). Mifepristone-inducible NIH3T3 stable cells expressing Flag-tagged MitoPLD were generated using the GeneSwitch system (Invitrogen) and MitoPLD was induced by treatment with 1 nM mifepristone (Invitrogen) for 16–24 h. For transfections, cells were grown on coverslips in 35-mm dishes (3–4 ± 10^5 cells per dish) and then switched into Opti-MEM I media before being transfected with 1 μg DNA per dish by using LipofectAMINE Plus. Two hours post-transfection, the media were replaced with fresh growth medium, and the cells incubated a further 20–24 h.

Western blotting. Mitochondrial lysates (20 Tg) were subjected to 12% SDS–PAGE and transferred to nitrocellulose membranes. The blots were probed with indicated primary antibodies, followed by secondary antibodies conjugated with Alexa 680 (Molecular Probes) or IRDye 800 (Rockland Immunochemicals, Gilbertsville, PA). Fluorescent signals were detected with an Odyssey infrared imaging system (LI-COR Biosciences, Lincoln, NB). Antibodies used in this study are as follows: anti-cytochrome *c* (Pharmingen, San Diego, CA), anti-Flag (M2; Sigma, St Louis, MO), anti-Hsp60 (Stressgen, San Diego, CA), anti-Smac (R&D Systems, Minneapolis, MN), anti-VDAC (Calbiochem, San Diego, CA), anti-TOM20 (FL-145, Santa Cruz, Santa Cruz, CA), anti-Mfn1 (see Supplementary Information, Methods), anti-Mfn2 (see Supplementary Information, Methods) and Alexa 488- or Alexa 647-conjugated secondary antibodies (Molecular Probes).

Quantitative real-time PCR. Total RNA was isolated from HeLa cells as indicated using an RNeasy Mini Kit (Qiagen, Valencia, CA) and reverse transcribed into single stranded cDNA using the 1st Strand cDNA Synthesis Kit for RT–PCR (AMV; Roche, Palo Alto, CA). Quantitative real-time PCR analysis was performed using the LightCycler system (Roche) and FastStart DNA Master SYBR Green I (Roche). Calculated concentrations of *MitoPLD* cDNA were normalized with respect to the expression level of glyceraldehyde-3-phosphate dehydrogenase (*GAPDH*) for each sample. Primers used for real time PCR were: human *GAPDH*, 5′-GAAGGTGAAGGTCGGAGTC-3′ (sense) and 5′-GAAGATGGTGATGGGATTTC-3′′ (antisense); human *MitoPLD*, 5′-CTCTGCCTGTTCGCCTTCT-3′ (sense) and 5′-CATTCTCCCTGTTGTTCTGG-3′ (antisense).

Tissue dot blot. Dot blotting was carried out using a human multiple tissue expression array (Clontech) as per manufacturer's instructions.

CLS complementation assay. *Saccharomyces cerevisiae cls* (YDL142C) and human *MitoPLD* genes were individually subcloned into pYES2 vectors (Invitrogen), and transformed separately into *cls* null yeast cells (MATα, *cls*, *ura3*, *leu2*, *met*). Subsequently, transformed yeast cells were labelled with 10 μCi ml^{-1} ^{3}H-palmitate, and CLS and MitoPLD protein expressions were induced by galactose for 14–16 h. Yeast cells were broken open with glass beads, and lipids were then extracted and analysed by thin layer chromatography, followed by autoradiography as described in the Supplementary Information, Methods. Positions of cardiolipin and phosphatidylglycerol spots were determined by standard lipids (Sigma) visualized by iodine staining.

***In vitro* cardiolipin PLD assay.** Recombinant bacmids were prepared by transformation of DH10Bac *Escherichia coli* cells with the pFastBac (Invitrogen) containing wild-type and mutant *MitoPLD* cDNAs C-terminally tagged with 6×His. Recombinant baculoviruses were amplified and propagated using standard procedures. Monolayer cultures of exponentially growing Sf9 cells were infected with baculoviruses at a multiplicity of 10 and were cultured for 48 h at 27 °C. The proteins were purified by Ni-NTA agarose (Qiagen), eluted using imidazole (250 mM), dialyzed against PBS, and quantitated using Coomassie Plus protein assay reagent (Pierce, Rockford, IL).

NIH3T3 cells (4 × 10^7) were labelled with 2 μCi ml^{-1} ^{3}H-palmitic acid (American Radiolabeled Chemicals, St Louis, MO) for 24 h, harvested and subjected to lipid extraction. The resulting lipids were separated by TLC, and silica corresponding to the retardation factor (Rf) value of a cardiolipin standard was scraped off of the TLC plate. Radiolabelled cardiolipin was extracted from the silica, mixed with bovine heart lipid extracts (150 μg; Avanti Polar Lipids, Alabaster, AL), dried down and resuspended in HEPES buffer (10 mM at pH 7.4) using sonication. The assay was performed at 37 °C for 30 min with cardiolipin (100,000 dpm), MitoPLD (500 ng) and assay buffer (50 mM HEPES at pH 7.5, 80 mM KCl, 1 mM DTT, 3 mM $MgCl_2$ and 2 mM $CaCl_2$) in a total volume of 100 μl. The reaction was stopped with CH_3OH:$CHCl_3$:0.1 M HCl (10:5:4, v/v) and the lipids recovered by acid organic extraction (half-volumes each of $CHCl_3$, 0.1 M HCl and 0.5 M NaCl). The organic fraction was dried down, dissolved in chloroform, and separated on a 10× 10-cm silica gel 60 HPTLC plate (EMD Chemicals, Gibbstown, NJ) using

chloroform:methanol:water:ammonium hydroxide (120:75:6:2, v/v) as the solvent. The position of phosphatidic acid and cardiolipin on the analysis plate was determined by matching the migration distances to cold standards run in parallel and was visualized using iodine staining.

Note: Supplementary Information is available on the Nature Cell Biology website.

ACKNOWLEDGMENTS

We thank U. Moll, C. Kisker, J. C. Hsieh, G. Rodomen, S. Van Horn, M. Fuller, M. Rojo, R. J. Youle, D. Bogenhagen, J. Vicogne, A. Neiman, G. Du, S. Tsirka and members of the Frohman lab for technical advice and assistance, reagents and critical discussions. The work was supported by awards National Institute of Diabetes and Digestive and Kidney Diseases (NIDDK; 64166) and National Institute of General Medical Sciences (NIGMS; 71520) to M.A.F., a National Research Service Award (NRSA) T32 fellowship to G.M.J., and a fellowship award to S.Y.C. from the United Mitochondrial Disease Foundation.

AUTHOR CONTRIBUTIONS

S.Y.C. and M.A.F. conceived the project. S.Y.C. performed most of the experiments with additional contributions from P.H., G.M.J. and J.S. D.C. provided *Mfn*-deficient cell lines and technical advice. The manuscript was mostly written by S.Y.C. and M.A.F.

COMPETING FINANCIAL INTERESTS

The authors declare that they have no competing financial interests.

Published online at http://www.nature.com/naturecellbiology/
Reprints and permissions information is available online at http://npg.nature.com/reprintsandpermissions

1. Bonifacino, J. S. & Glick, B. S. The mechanisms of vesicle budding and fusion. *Cell* **116,** 153–166 (2004).
2. Weber, T. *et al.* SNAREpins: minimal machinery for membrane fusion. *Cell* **92,** 759–772 (1998).
3. Vitale, N. *et al.* Phospholipase D1: a key factor for the exocytotic machinery in neuroendocrine cells. *EMBO J.* **20,** 2424–2434 (2001).
4. Huang, P., Altshuller, Y. M., Chunqiu Hou, J., Pessin, J. E. & Frohman, M. A. Insulin-stimulated plasma membrane fusion of Glut4 glucose transporter-containing vesicles is regulated by phospholipase D1. *Mol. Biol. Cell* **16,** 2614–2623 (2005).
5. Di Paolo, G. *et al.* Impaired PtdIns(4,5)P2 synthesis in nerve terminals produces defects in synaptic vesicle trafficking. *Nature* **431,** 415–422 (2004).
6. Hales, K. G. & Fuller, M. T. Developmentally regulated mitochondrial fusion mediated by a conserved, novel, predicted GTPase. *Cell* **90,** 121–129 (1997).
7. Malka, F. *et al.* Separate fusion of outer and inner mitochondrial membranes. *EMBO Rep.* **6,** 853–859 (2005).
8. Meeusen, S., McCaffery, J. M. & Nunnari, J. Mitochondrial fusion intermediates revealed in vitro. *Science* **305,** 1747–1752 (2004).
9. Koshiba, T. *et al.* Structural basis of mitochondrial tethering by mitofusin complexes. *Science* **305,** 858–862 (2004).
10. Ishihara, N., Eura, Y. & Mihara, K. Mitofusin 1 and 2 play distinct roles in mitochondrial fusion reactions via GTPase activity. *J. Cell Sci.* **117,** 6535–6546 (2004).
11. Nakanishi, H. *et al.* Phospholipase D and the SNARE Sso1p are necessary for vesicle fusion during sporulation in yeast. *J. Cell. Sci.* **119,** 1406–1415 (2006).
12. Hammond, S. M. *et al.* Human ADP-ribosylation factor-activated phosphatidylcholine-specific phospholipase D defines a new and highly conserved gene family. *J. Biol. Chem.* **270,** 29640–29643 (1995).
13. Sung, T. C. *et al.* Mutagenesis of phospholipase D defines a superfamily including a trans- Golgi viral protein required for poxvirus pathogenicity. *EMBO J.* **16,** 4519–4530 (1997).
14. Stuckey, J. A. & Dixon, J. E. Crystal structure of a phospholipase D family member. *Nature Struct. Biol.* **6,** 278–284 (1999).
15. Kanaji, S., Iwahashi, J., Kida, Y., Sakaguchi, M. & Mihara, K. Characterization of the signal that directs Tom20 to the mitochondrial outer membrane. *J. Cell Biol.* **151,** 277–288 (2000).
16. Leiros, I., Secundo, F., Zambonelli, C., Servi, S. & Hough, E. The first crystal structure of a phospholipase D. *Structure Fold Des.* **8,** 655–667 (2000).
17. Legros, F., Lombes, A., Frachon, P. & Rojo, M. Mitochondrial fusion in human cells is efficient, requires the inner membrane potential, and is mediated by mitofusins. *Mol. Biol. Cell* **13,** 4343–4354 (2002).
18. Chen, H. *et al.* Mitofusins Mfn1 and Mfn2 coordinately regulate mitochondrial fusion and are essential for embryonic development. *J. Cell Biol.* **160,** 189–200 (2003).
19. Chen, H., Chomyn, A. & Chan, D. C. Disruption of fusion results in mitochondrial heterogeneity and dysfunction. *J. Biol. Chem.* **280,** 26185–26192 (2005).
20. Cable, M. B., Jacobus, J. & Powell, G. L. Cardiolipin: a stereospecifically spin-labeled analogue and its specific enzymic hydrolysis. *Proc. Natl Acad. Sci. USA* **75,** 1227–1231 (1978).
21. Liu, J. *et al.* Phospholipid scramblase 3 controls mitochondrial structure, function, and apoptotic response. *Mol. Cancer Res.* **1,** 892–902 (2003).
22. Hovius, R., Thijssen, J., van der Linden, P., Nicolay, K. & de Kruijff, B. Phospholipid asymmetry of the outer membrane of rat liver mitochondria. Evidence for the presence of cardiolipin on the outside of the outer membrane. *FEBS Lett.* **330,** 71–76 (1993).
23. Cao, J., Liu, Y., Lockwood, J., Burn, P. & Shi, Y. A novel cardiolipin-remodeling pathway revealed by a gene encoding an endoplasmic reticulum-associated acyl-CoA:lysocardiolipin acyltransferase (ALCAT1) in mouse. *J. Biol. Chem.* **279,** 31727–31734 (2004).
24. Karbowski, M. *et al.* Quantitation of mitochondrial dynamics by photolabeling of individual organelles shows that mitochondrial fusion is blocked during the Bax activation phase of apoptosis. *J. Cell Biol.* **164,** 493–499 (2004).
25. Esposti, M. D., Cristea, I. M., Gaskell, S. J., Nakao, Y. & Dive, C. Proapoptotic Bid binds to monolysocardiolipin, a new molecular connection between mitochondrial membranes and cell death. *Cell Death. Differ.* **10,** 1300–1309 (2003).
26. Kagan, V. E. *et al.* Cytochrome *c* acts as a cardiolipin oxygenase required for release of proapoptotic factors. *Nature Chem. Biol.* **1,** 223–232 (2005).
27. Neutzner, A. & Youle, R. J. Instability of the mitofusin Fzo1 regulates mitochondrial morphology during the mating response of the yeast *Saccharomyces cerevisiae*. *J. Biol. Chem.* **280,** 18598–18603 (2005).
28. Nakanishi, H., de los Santos, P. & Neiman, A. M. Positive and negative regulation of a SNARE protein by control of intracellular localization. *Mol. Biol. Cell* **15,** 1802–1815 (2004).
29. Vicogne, J. *et al.* Asymmetric phospholipid distribution drives *in vitro* reconstituted SNARE-dependent membrane fusion. *Proc. Natl Acad. Sci. USA* doi: 10.1073/pnas0606881103 (2006).
30. Zuchner, S. *et al.* Mutations in the mitochondrial GTPase mitofusin 2 cause Charcot-Marie-Tooth neuropathy type 2A. *Nature Genet.* **36,** 449–451 (2004).
31. Kuhlenbaumer, G., Young, P., Hunermund, G., Ringelfstein, B. & Stogbauer, F. Clinical features and molecular genetics of hereditary peripheral neuropathies. *J. Neurol.* **249,** 1629–1650 (2002).

a.

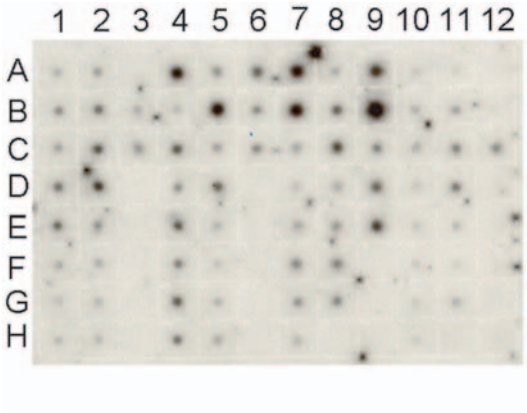

	1	2	3	4	5	6	7	8	9	10	11	12
A	whole brain	cerebellum, left		heart	esophagus	colon, transverse	kidney	lung	liver	leukemia, HL-60	fetal brain	yeast total RNA
B	cerebral cortex	cerebellum, right	accumbens nucleus	aorta	stomach	colon, desending	skeletal muscle	placenta	pancreas	HeLa S3	fetal heart	yeast tRNA
C	frontal lobe	corpus callosum	thalamus	atrium, left	duodenum	rectum	spleen	bladder	adrenal gland	leukemia, K-562	fetal kidney	*E. coli* rRNA
D	parietal lobe	amygdala		atrium, right	jejunum		thymus	uterus	thyroid gland	leukemia, MOLT-4	fetal liver	*E. coli* DNA
E	occipital lobe	caudate nucleus		ventricle, left	ileum		peripheral blood leukocyte	prostate	salivary gland	Burkitt's lymphoma, Raji	fetal spleen	Poly r(A)
F	temporal lobe	hippo-campus		ventricle, right	ilocecum		lymph node	testis		Burkitt's lymphoma, Daudi	fetal thymus	human $C_{o}t$ -1 DNA
G	p. g.* of cerebral cortex	medulla oblongata		inter-ventricular septum	appendix		bone marrow	ovary		colorectal adeno-carcinoma, SW480	fetal lung	human DNA 100 ng
H	pons	putamen		apex of the heart	colon, ascending		trachea			lung carcinoma, A549		human DNA 500 ng

* paracentral gyrus

b.

```
                    Mitochondrial Localization Sequence / TM domain  ▽                  67
Human                     MGRLSWQVAA AAAVGLALTL EALPWVLRW- LRSRRRRPRR --EAPFFPSQ VTCTEALLRA PGAELAELPE
Mouse                     MGRSSWRLVF AAGAGLALAL EALPWLMRW- LLAGRR-PRR --EVLFFPSQ VTCTEALLQA PG--LPPGPS
Drosophila          MLITQIIMKQ IRDYPIVSTI SIAVSTVLAS EVIWKLVQC- SRSKREKASR VHEVIIFNEL GEICAAVHMR NSSMGSQKPQ
E. coli CLS         MVDPRYFKQD AGVGQWIDLM ARMEGPIATA MGIIYSCDWE IETGKRILPP PPDVNIMPFE QASGHTIHTI ASG------P
Salmonella Nuc                                                          MKKL ATWLLAAAFT TAALPAFAVE

                                                    RGV motif                          143
Human               GCPCGLPH-G ESALSRLLRA LLAARASLDL CLFAFSSPQL GHAVQLLHQR GVRVRVV--- TDCDYMALNG SQIGLLRKAG
Mouse               GCPCSLPH-S ESSLSRLLRA LLAARSSLEL CLFAFSSPQL GRAVQLLHQR GVRVRVI--- TDCDYMALNG SQIGLLRKAG
Drosophila          VSPCCNTHCS LRNVAKIVEQ IDRAVYSIDL AIYTFTSLFL ADSIKRALQR GVIIRII--- SDGEMVYSKG SQISMLAQLG
E. coli CLS         GFPEDLIH-- ---QALLTAA YSAREYLIMT TPYFVPSDDL LHAICTAAQR GVDVSIILPR KNDSMLVGWA SRAFFTELLA
Salmonella Nuc      PSVQVGYSPE GSARVLVLSA IDSAKTSIRM MAYSFTAPDI MKALVAAKKR GVDVKIVIDE RGNTGRASIA A-MNYIANSG

                  HKD motif: H K      D                                GS  N                 201
Human               IQVR-HDQDP GYMHHKFAIV DK-------- ---------- --RVLITGSL NWTTQAIQNN RENVLITED- DEYVRLFLEE
Mouse               IQVR-HDQDL GYMHHKFAIV DK-------- ---------- --KVLITGSL NWTTQAIQNN RENVLIMED- TEYVRLFLEE
Drosophila          VPVR-VPITT NLMHNKFCII DGFERVEEIR LLRKLKFMRP CYSIVISGSV NWTALGLGGN WENCIITAD- DKLTATFQAE
E. coli CLS         AGVKIYQFEG GLLHTKSVLV DG-------- ---------- --ELSLVGTV NLDMRSLWLN FEITLAIDD- KGFGADLAAV
Salmonella Nuc      IPLR-TDSNF PIQHDKVIIV DN-------- ---------- --VTVETGSF NFTKAAETKN SENAVVIWNM PKLAESFLEH

                                                                                    252
Human               FERIWEQFNP TKYTFFPPKK SHGSCAPPVS RAGGRLLSWH RTCGTSSESQ T
Mouse               FERIWEEFDP TKYSFFPQKH RGH
Drosophila          FQRMWRAFAK TEGSQIQLK
E. coli CLS         QDDYISRSRL LDARLWLKRP LWQRVAERLF YFFSPLL
Salmonella Nuc      WQDRWNQGRD YRSSY
```

Figure S1 MitoPLD expression pattern and sequence comparisons. **(a)** A human multiple tissue expression array (Clontech) was hybridized with a [^{32}P]-labeled human MitoPLD probe spanning the open reading frame. Shown on the right are the sources of mRNAs used in the array. **(b)** Multiple sequence alignment of human (AAH31263), mouse (CAI24298), and *Drosophila melanogaster* (NP_609530) MitoPLDs, *Salmonella typhimurium* Nuc (AAL13395) and *E. coli* cardiolipin synthase (NP_753618). Only the C-terminal half of *E. coli* CLS (aa 242-481) was aligned. The box and open triangle respectively indicate the mitochondrial localization sequence (MLS) and cleavage site predicted for human MitoPLD protein by the MITOPROT program (http://ihg.gsf.de/ihg/mitoprot.html), which estimated a 78% probability that MitoPLD would localize to mitochondria. MLSs are generally amphipathic and positively charged; the MitoPLD MLS is amphipathic and contains 9 positively-charged residues and 1 negative charged residue. However, these guidelines refer primarily to imported proteins, which we show later does not appear to take place for MitoPLD, so the computer prediction is of less significance in this instance. Amino acid residues 5-27 (numbering according to the human sequence) were alternately predicted to function as a transmembrane helix by the TMHMM program (http://www.cbs.dtu.dk/services/TMHMM/). Other regions of interest are underlined. Red indicates highly conserved amino acid residues. Blue represents less highly conserved residues. TM, transmembrane; CLS, cardiolipin synthase. The RGV motif has not previously been described and its function is currently unknown; it could play a role in protein:protein or protein:lipid interactions since it lies at the back of the enzyme with respect to the active site (see Fig. 1h). The human MitoPLD gene localizes to human chromosome 17p11.2.

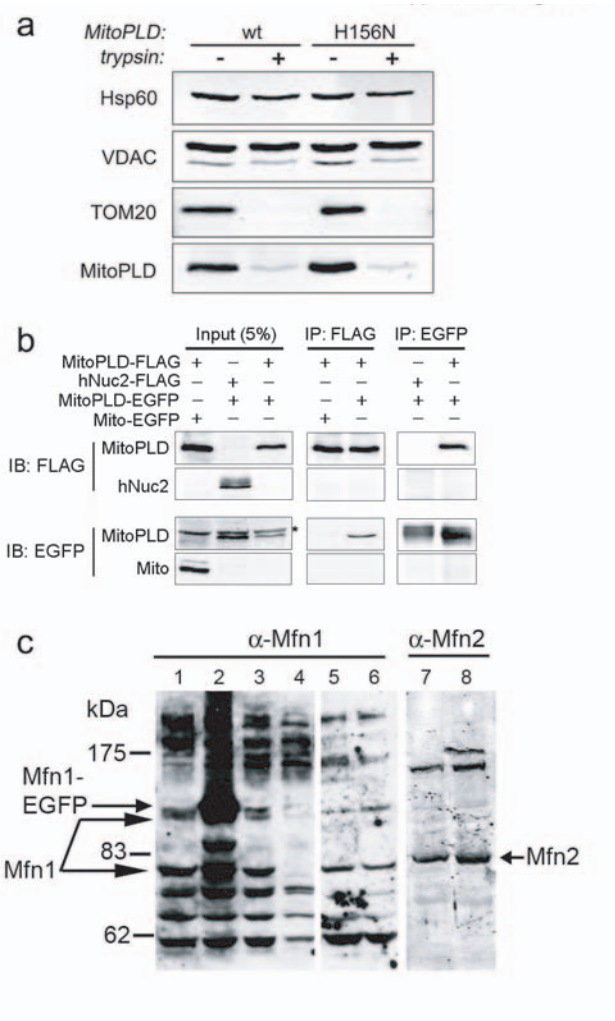

Figure S2 MitoPLD topology as determined by surface digestion using Trypsin, and lack of protein:protein interaction of MitoPLD with Mfn or effects of MitoPLD deficiency on Mfn expression. **(a)** Topology. Mitochondria purified from cells expressing FLAG-tagged wt or H156N MitoPLD were exposed to trypsin. Hsp60 (a mitochondrial matrix protein), VDAC (an integral outer membrane protein), and TOM20 (which projects from the outer membrane) were visualized using commercial antisera. **(b)** Co-IP. NIH3T3 cells were transiently co-transfected with plasmids for FLAG- and EGFP-tagged MitoPLD or control plasmids as indicated (hNuc2 is another presently uncharacterized HKD-containing gene that exhibits sequence similarity to bacterial Nuc but does not localize to mitochondria, unpublished data; Mito-EGFP is EGFP fused to the MLS of subunit VIII of human cytochrome C oxidase). Twenty-four hours post-transfection, the cells were lysed using 0.5% NP-40 in PBS, sonicated, and centrifuged at 13K x g for 5 min at 4ºC. The resulting supernatants were incubated with anti-EGFP (Abcam) or anti-FLAG (Sigma) antibodies in the presence of protein G-agarose (Sigma). The agarose was washed in lysis buffer, and the bound proteins were eluted using SDS loading buffer, subjected to 12% SDS-PAGE, transferred to nitrocellulose membranes and detected with an Odyssey infrared imaging system using the antibodies indicated. IP indicates antibody used for immunoprecipitation; IB indicates antibody used for western blot immunodetection. Asterisk indicates non-specific band detected by anti-EGFP antibody. Examination of the Input lanes indicates that all of the proteins were expressed at approximately equivalent levels. When FLAG-tagged MitoPLD was co-expressed with EGFP-tagged MitoPLD and immunoprecipated using either anti-FLAG or anti-EGFP antibody, the partner protein (EGFP-tagged MitoPLD or FLAG-tagged MitoPLD, respectively) was readily detected by western blot analysis. However, the partner proteins were not co-immunoprecipitated by Mito-EGFP or by hNuc2-FLAG, demonstrating specificity of the immunoprecipitation and detection reactions.**(c)** Mfn1 and 2 levels of expression are not altered in MitoPLD RNAi-targeted cells. Western blot analysis of parental cells, cells expressing tagged Mfn proteins, and control or MitoPLD RNAi-targeted cells were subjected to Western blot analysis using polyclonal antisera directed against Mfn1 and Mfn 2 with previously described protocols (4, 10). Left, Mfn1 analysis: In Lane 1, the parental NIH3T3 cells, many immunoreacting bands are observed. In Lane 2, a larger band is observed, indicating transiently-expressed EGFP-Mfn1 and demonstrating that the antibody does recognize Mfn1. Breakdown products, including one at approximately 80 kDa, which is close to the predicted size of Mfn1 (84 kDa), are also observed. In Lane 3, the antibody fails to recognize transiently EGFP-tagged Mfn2, demonstrating that it is isoform-specific. In lane 4, examination of mouse embryonic fibroblasts lacking Mfn1 indicates the disappearance of multiple immunoreactive bands – a major one migrating at approximately 80 kDa, a doublet almost as intense at approximately 110 kDa, and possibly several higher molecular weight bands (probably indicating incomplete denaturation and /or reassociation with other hydrophobic proteins during electrophoresis). Regardless, no difference in the level of Mfn1 is observed for the major band at 80 kDa between HeLa cells targeted using RNAi directed against Luciferase (Lane 5) versus ones targeted against MitoPLD (Lane 6). Similarly, no difference in the level of Mfn2 is observed between for the Luc (lane 7) or MitoPLD (Lane 8) RNAi targeted cell lines. Note – lanes 1-6 all derive from the same experiment and autorad, however, several non-relevant intervening lanes were excised from the figure between lanes 4 and 5. Lanes 7-8 derive from a separate western blot experiment.

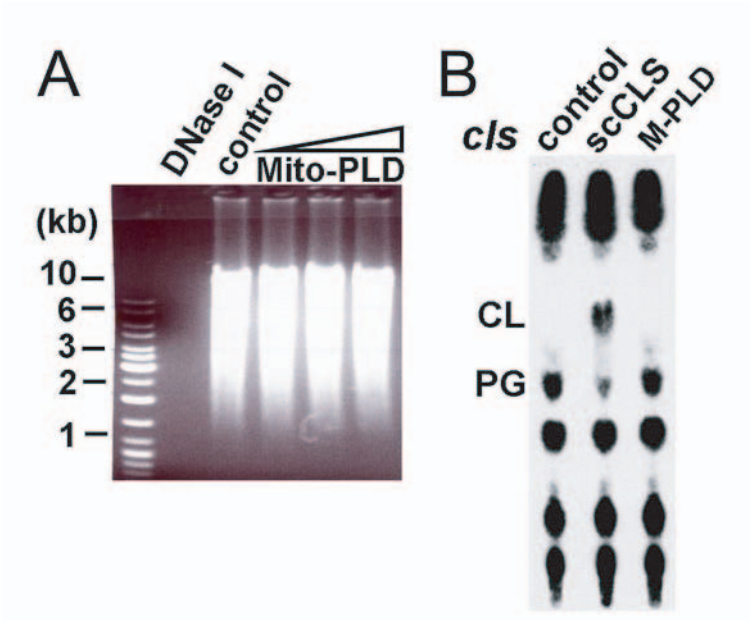

Figure S3 Neither nuclease nor CL synthetic activity can be detected for MitoPLD**. (a)** HeLa cell nuclear extract (200 μg) was incubated with either PBS (control), DNase I (10 unit) or MitoPLD overexpressing mitochondrial lysates (3 μg, 6 μg, 12 μg) for 2 hr at 37^°C. Nuclear DNA was precipitated by ethanol, resuspended, and electrophoresed on a 1% agarose gel. Shown on the left are DNA standards. (**b)** *S. cerevisiae* cells lacking cardiolipin synthase (YDL142C-3b, *crd1Δ*) were transformed with either a control vector or plasmids for the inducible expression of *S. cerevisiae* cardiolipin synthase (scCLS) or MitoPLD, labeled with [^{3}H]-palmitate, induced by galactose and processed for lipid extraction. Extracted lipids were separated by thin layer chromatography and visualized by autoradiography. CL, cardiolipin; PG, phosphatidylglycerol.

SUPPLEMENTAL INFORMATION, ADDITIONAL METHODS

SPLIT VENUS COMPLEMENTATION

The MitoPLD open reading frame was subcloned in frame and N-terminal to N- or C-terminal fragments of Venus fluorescent protein in a CMV-driven expression vector [1]. The resulting constructs were then co-transfected into NIH3T3 cells. The cells were incubated at 37^{o}C for 24 hr, stained with MitoTracker Deep Red 633 for 30 min, fixed and visualized using confocal microscopy. Neither expression plasmid generated detectable yellow fluorescence when expressed alone or with control non-interacting proteins.

MITOCHONDRIAL FRACTIONATIONS

Mitochondria were prepared by sucrose density gradient as described previously [2,3]. In brief, cells (5×10^7) were washed in TD buffer (135 mM NaCl, 5 mM KCl, 25 mM Tris-Cl, pH 7.6), swollen for 10 min in ice-cold hypotonic CaRSB buffer (10 mM NaCl, 1.5 mM CaCl2, 10 mM Tris-Cl, pH 7.5, protease inhibitors), and then disrupted in a glass Dounce homogenizer with 7-12 strokes. Subsequently, MS buffer (210 mM mannitol, 70 mM sucrose, 5 mM EDTA, 20 mM HEPES, pH 8.0) was added to stabilize mitochondria and nuclear contaminants removed by centrifugation (2 × 2,000 ***g*** for 5 min). The resulting supernatant was layered on top of a 1.0 M sucrose over 1.5 M sucrose step gradient (in 20 mM HEPES, pH 8.0, 2 mM EDTA, 2 mM dithiothreitol, protease inhibitors) and spun at 4 °C for 35 min at 85,000 ***g***. Mitochondria were collected at the 1-1.5 M interphase by lateral suction through the tube, washed (in 5 volumes of MS buffer), spun (for 20 min at 16,000 ***g***), resuspended in MS buffer, and used for all assays.

PROTEOLYTIC STRIPPING OF MITOCHONDRIA

Freshly isolated mitochondria (2 mg/ml in MS buffer) were incubated with Proteinase K (10 μg/ml, Roche) in the absence or presence of Triton X-100 (0.5%, Sigma) at 4 °C for 30 min, or with trypsin (10 μg/ml) at 37°C for 30 min. Digestions were stopped by the addition of PMSF (2 mM, Sigma) and SDS loading buffer and boiling at 95°C for 5 min.

MITOCHONDRIAL FUSION ASSAY

Mitochondrial fusion assays were carried out as described previously [4]. In brief, individual pools of cells respectively expressing mitochondrially-targeted EGFP and DsRed2 (Clontech) were mixed and plated on poly-L-lysine pretreated coverslips 12 h before cell fusion. Cycloheximide (20 μg/ml) was added 30 min before fusion and kept thereafter. The cells were incubated with 50% PEG (polyethylene glycol) 1500 (Roche) for 60 sec, washed four times with complete media, grown for 7 hrs and then fixed.

GENERATION OF HELA CELLS STABLY EXPRESSING shRNA.

A 19-nucleotide (nt) sequence, nt 2351-2369 (GCCAGCTTGGAAGTTAACT) matching human MitoPLD mRNA (GenBank accession number NM_178836) was chosen to perform MitoPLD RNAi targeting. Small hairpin (sh) RNAs were synthesized as complementary DNA oligonucleotides, annealed, and cloned into the *Bgl*II/*Acc65*I sites of a modified pSUPER vector [5] containing a blasticidin resistance gene. The resulting plasmids were transfected into HeLa cells using LipofectAMINE Plus and stably-transfected cells selected by blasticidin (10 μg/ml). An siRNA sequence corresponding to nt 1235–1253 (GATTTCGAGTCGTCTTAAT) of the *Photinus pyralis* (firefly) luciferase mRNA (GenBank accession number M15077) was used as a negative control.

PHOSPHOLIPID ANALYSIS

NIH3T3 cells were labeled with 2 μCi/ml [^{3}H] palmitic acid (American Radiolabeled Chemicals) for 24 h. The mitochondria were then isolated as described in the "Mitochondrial Fractionations" section. Mitochondrial pellets were homogenized in $CH_3OH/CHCl_3$/0.1 N HCl (10:5:4, v/v) and the lipids recovered by acid organic extraction (half-volumes each of $CHCl_3$, 0.1 N HCl, and 0.5 M NaCl) [6]. An organic fraction was dried down, dissolved in chloroform, and separated on a 10 x 10-cm silica gel 60 HPTLC plate (EMD Chemicals) either one-dimensionally using chloroform/methanol/water/ammonium hydroxide (120:75:6:2, v/v) as the solvent [7] or

two-dimensionally using chloroform/methanol/water (32.5:12.5:2, v/v) for the first dimension and chloroform/acetone/methanol/acetic acid/water (6:8:2:2:1, v/v) in the second direction [8]. The plate was sprayed with EN^{3}HANCE (PerkinElmer Life and Analytical Sciences) and exposed to x-ray film (BioMax MR, Kodak) for 2 days at -80 °C.

IN VITRO *DNASE ASSAY*

The DNA fragmentation was assayed by incubating HeLa cell nuclei with lysates of mitochondria overexpressing MitoPLD at 37°C for 2 hr using a method described previously [9].

IMMUNOFLUORESCENCE STAINING

Unless stated otherwise, cells were fixed with 3% paraformaldehyde for 15 min, permeabilized with 0.2% Triton X-100, and blocked with 5% normal goat serum. The cells were then immunostained using primary antibodies against the specific proteins, followed by fluorescent dye-conjugated secondary antibodies. Stained cells were visualized using a Leica TCS SP2 confocal microscope. Images were processed using Adobe Photoshop 7.0, and quantitative analyses were performed using the ImageJ analysis software package (National Institutes of Health). All experiments were performed at least three times with similar results.

ESTIMATION OF MITOCHONDRIAL MEMBRANE POTENTIAL ($\Delta\Psi_m$).

NIH3T3 cells were transfected with MitoPLD-EGFP. Twenty-four hours post-transfection, cells were incubated with 100 nM TMRE (Molecular Probes) at 37 °C for 20 min, washed, and visualized by a Leica TCS SP2 confocal microscope equipped with a bipolar temperature controller (Harvard Apparatus).

ELECTRON MICROSCOPY

NIH3T3 cells were fixed in 2% paraformaldehyde and 2.5% glutaraldehyde, stained sequentially in 2% OsO_4 and 1% uranyl acetate, dehydrated by a series of ethanol washes and embedded in Spurr resin for sectioning and analysis. Samples were analyzed with the use of a JEOL 1200EX transmission electron microscope at the Stony Brook University Microscopy Imaging Center.

Supplemental References.

1. Hu, C. D., Chinenov, Y. & Kerppola, T. K. Visualization of interactions among bZIP and Rel family proteins in living cells using bimolecular fluorescence complementation. Mol Cell 9, 789-98 (2002). See also: Shyu, Y. J., Liu, H., Deng, X. & Hu, C. D. Identification of new fluorescent protein fragments for bimolecular fluorescence complementation analysis under physiological conditions. Biotechniques 40, 61-6 (2006).
2. Marchenko, N. D., Zaika, A. & Moll, U. M. Death signal-induced localization of p53 protein to mitochondria. A potential role in apoptotic signaling. J Biol Chem 275, 16202-12 (2000).
3. Bogenhagen, D. & Clayton, D. A. The number of mitochondrial deoxyribonucleic acid genomes in mouse L and human HeLa cells. Quantitative isolation of mitochondrial deoxyribonucleic acid. J Biol Chem 249, 7991-5 (1974).
4. Legros, F., Lombes, A., Frachon, P. & Rojo, M. Mitochondrial fusion in human cells is efficient, requires the inner membrane potential, and is mediated by mitofusins. Mol Biol Cell 13, 4343-54 (2002).
5. Brummelkamp, T. R., Bernards, R. & Agami, R. A system for stable expression of short interfering RNAs in mammalian cells. Science 296, 550-3 (2002).
6. Ostrander, D. B., Sparagna, G. C., Amoscato, A. A., McMillin, J. B. & Dowhan, W. Decreased cardiolipin synthesis corresponds with cytochrome c release in palmitate-induced cardiomyocyte apoptosis. J Biol Chem 276, 38061-7 (2001).
7. Bektas, M. et al. A novel acylglycerol kinase that produces lysophosphatidic acid modulates cross talk with EGFR in prostate cancer cells. J Cell Biol 169, 801-11 (2005).
8. Schlame, M. & Rustow, B. Lysocardiolipin formation and reacylation in isolated rat liver mitochondria. Biochem J 272, 589-95 (1990).

9. Liu, X., Zou, H., Slaughter, C. & Wang, X. DFF, a heterodimeric protein that functions downstream of caspase-3 to trigger DNA fragmentation during apoptosis. Cell 89, 175-84 (1997).
10. Chen, H. et al. Mitofusins Mfn1 and Mfn2 coordinately regulate mitochondrial fusion and are essential for embryonic development. J Cell Biol 160, 189-200 (2003).